Solution-Processible Organic Semiconductors Based on Selenophene-Containing Heteroarenes, 2,7-Dialkyl[1]benzoselenopheno[3,2-*b*][1]benzoselenophenes (C_n-BSBSs): Syntheses, Properties, Molecular Arrangements, and Field-Effect Transistor Characteristics

Takafumi Izawa,[†] Eigo Miyazaki,[†] and Kazuo Takimiya*[,†,‡]

Department of Applied Chemistry, Graduate School of Engineering, Hiroshima University, Higashi-Hiroshima 739-8527, Japan, and Institute for Advanced Materials Research, Hiroshima University, Higashi-Hiroshima 739-8530, Japan

Received November 6, 2008. Revised Manuscript Received December 19, 2008

A series of 2,7-dialkyl[1]benzoselenopheno[3,2-*b*][1]benzoselenophenes (C_n-BSBSs) were synthesized as novel soluble organic semiconductors. Electrochemical and photochemical studies on C_n-BSBSs have revealed that their molecular properties are very similar to those of their sulfur counterparts, 2,7-dialkyl[1]benzothieno[3,2-*b*][1]benzothiophenes (C_n-BTBTs), whose solution-processed organic field-effect transistors (OFETs) show superior FET characteristics with field-effect mobility (μ_{FET}) higher than 1.0 $cm^2\ V^{-1}\ s^{-1}$. Thin film deposition of C_n-BSBSs on Si/SiO_2 substrates was easily accomplished by physical vapor deposition or spin-coating of their solutions in chloroform. Atomic force microscopy (AFM) showed that the thin films, regardless of the alkyl chain length and the deposition method, consist of crystalline grains. X-ray diffraction (XRD) measurements, on the other hand, indicated that all the thin films on the substrate have a well-ordered "molecular lamella" structure where C_n-BSBS molecules have an edge-on orientation on the substrate, as observed in the thin films of C_n-BTBTs. However, the short intermolecular distances (*d*-spacings) of C_n-BSBS thin films compared to those of C_n-BTBT thin films with the same alkyl chain length correspond to the large inclination of the molecular long axis from the substrate normal, indicating that the intermolecular overlap between the BSBS cores is less effective than that for the two-dimensional interactive structure observed for C_n-BTBT thin films. In accordance with the molecular arrangement and the resulting less interactive electronic structure of C_n-BSBS thin films, the characteristics of C_n-BSBS-based OFETs were less remarkable than those of C_n-BTBT-based ones, although the maximum μ_{FET} of 0.23 $cm^2\ V^{-1}\ s^{-1}$ with $I_{on/off}$ of 10^5 was achieved. The results indicate that even subtle molecular modifications without significant changes of the molecular electronic structure could alter the molecular arrangement in the solid state, which would result in a large difference in device characteristics. For the further development of superior organic semiconductors, not only the molecular electronic structure but also the electronic structure in the solid state must be taken into account.

Introduction

Since the past decade, organic semiconductors have been receiving significant attention as a new class of electronic materials for organic light emitting diodes (OLEDs), organic field-effect transistors (OFETs), and photovoltaic cells.[1] Among those devices, OFETs are attracting much interest for their potential application to radio frequency identification tags (RFIDs), driving circuits of bendable displays, and low-cost memories and sensors.[2] To differentiate the technologies based on organic semiconductors from those based on conventional inorganic semiconductors, the solution-based deposition of semiconducting layers using casting, spin-coating, or printing techniques to realize low-cost and large-area fabrication of electronic devices is of primary importance.[3] Great effort has been devoted to the development of solution-processible organic semiconductors and the fabrication techniques for solution-processed OFETs. Conventional soluble organic semiconductors amenable to solution processes include conjugated polymers or oligomers represented by poly(3-alkylthiophenes),[3] and recent modifications of the polymer structure as well as improvements of the fabrication

* Corresponding author. E-mail: ktakimi@hiroshima-u.ac.jp.
† Department of Applied Chemistry.
‡ Institute for Advanced Materials Research.

(1) (a) *Thin-Film Transistors*; Kagan, C. R., Andry, P. Eds.; Marcel Dekker: New York, 2003, p 377. (b) *Organic Electronics, Manufacturing and Applications*; Klauk, H., Ed.; Wiley-VCH: Weinheim, 2006. (c) See also a special issue on organic electronics: Jenkhe, S. A. *Chem. Mater.* **2004**, *16*, 4381–4846.

(2) For recent reviews on this topic, see: (a) Katz, H. E.; Bao, Z.; Gilat, S. L. *Acc. Chem. Res.* **2001**, *34*, 359–369. (b) Dimitrakopoulos, C. D.; Malenfant, R. L. *Adv. Mater.* **2002**, *14*, 99–117. (c) Horowitz, G. *J. Mater. Res.* **2004**, *19*, 1946–1962. (d) Newman, C. R.; Frisbie, C. D.; daSilvaFilho, D. A.; Bredas, J. L.; Ewbank, P. C.; Mann, K. R. *Chem. Mater.* **2004**, *16*, 4436–4451. (e) Katz, H. E. *Chem. Mater.* **2004**, *16*, 4748–4756. (f) Sirringhaus, H. *Adv. Mater.* **2005**, *17*, 2411–2425. (g) Anthony, J. E. *Chem. Rev.* **2006**, *106*, 5028–5048. (h) Murphy, A. R.; Frechet, J. M. J. *Chem. Rev.* **2007**, *107*, 1066–1096. (i) Takimiya, K.; Kunugi, Y.; Otsubo, T. *Chem. Lett.* **2007**, *36*, 578–583. (j) Mas-Torrent, M.; Rovira, C. *Chem. Soc. Rev.* **2008**, *37*, 827–838.

10.1021/cm8030126 CCC: $40.75
Published on Web 02/04/2009

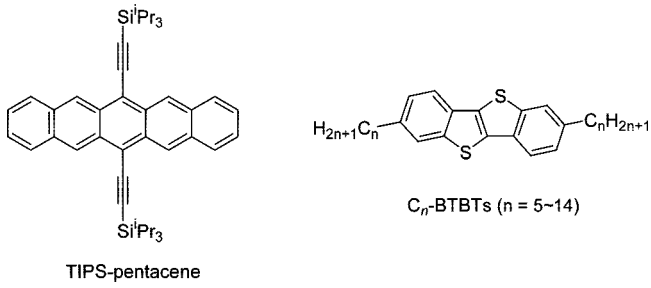

Figure 1. High-performance soluble molecular semiconductors.

techniques[4] have led to the realization of high-performance solution-processed OFETs showing field-effect mobility (μ_{FET}) higher than 1.0 cm^2 V^{-1} s^{-1}.[5]

Meanwhile, soluble molecular semiconductors are also currently attracting interest.[6] Among such molecular semiconductors, 6,13-bis(triisopropylsilylethynyl)pentacene (TIPS-pentacene, Figure 1) developed by Anthony et al. is a prime example, and FET devices fabricated with its solution-cast films showed μ_{FET} as high as 1.8 cm^2 V^{-1} s^{-1}.[7]

Another example of high-performance solution-processed OFETs with molecular semiconductors is the device based on 2,7-dialkyl[1]benzothieno[3,2-*b*][1]benzothiophenes (C_n-BTBTs, Figure 1), which shows μ_{FET} of up to 2.7 cm^2 V^{-1} s^{-1}.[8] The high performance of C_n-BTBT-based OFETs is due to their well-ordered molecular array in the thin film state: not only the intermolecular interaction between heteroarene cores but also the hydrophobic intermolecular interaction between alkyl chains serves to enhance molecular orbital overlap between neighboring molecules, which can enhance carrier mobility in the devices.[9]

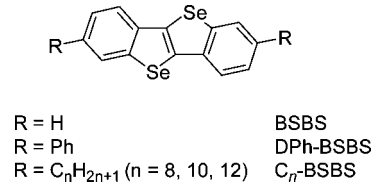

Figure 2. BSBS derivatives.

For the further enhancement of intermolecular overlap, one potential molecular modification is the substitution of sulfur atoms in C_n-BTBTs with selenium atoms that have larger atomic radius and higher polarizability than the sulfur atoms. Actually, a few selenophene-containing organic semiconductors[10] as well as related electronic materials[11] were recently developed. Thus, we focused on the selenium counterparts of C_n-BTBTs, namely, 2,7-dialkyl[1]benzoselenopheno[3,2-*b*][1]benzoselenophenes (C_n-BSBSs, Figure 2), as new candidates for high-performance soluble organic semiconductors.

From the viewpoint of synthetic chemistry, however, the preparation of selenophene-containing materials is always more difficult than the preparation of their thiophene counterparts. This is due to the lack of starting materials, reagents, and key intermediates, as well as the limited synthetic reactions and methodologies.[12] Therefore, we started studies on C_n-BSBSs from synthetic trials and were able to establish an efficient route to a series of C_n-BSBSs (n = 8, 10, 12, 14) that are sufficient for further studies on the fabrication/evaluation of the thin film state. In this article, we report a new synthetic route for C_n-BSBSs using 2,7-dibromo-BSBS as the key intermediate. We also report the results of single-crystal X-ray structural analysis, the thin film structure, and the FET characteristics of C_n-BSBSs (n = 8, 10, 12, 14).

Results

Synthesis. The parent BSBS has long been known since 1972 when Faller and Mantovani isolated BSBS as a

(3) (a) Bao, Z.; Dodabalapur, A.; Lovinger, A. J. *Appl. Phys. Lett.* **1996**, *69*, 4108–4110. (b) Sirringhaus, H.; Wilson, R. J.; Friend, R. H.; Inbasekaran, M.; Wu, W.; Woo, E. P.; Grell, M.; Bradley, D. D. C. *Appl. Phys. Lett.* **2000**, *77*, 406–408. (c) Ong, B. S.; Wu, Y.; Liu, P.; Gardner, S. *J. Am. Chem. Soc.* **2004**, *126*, 3378–3379. (d) Heeney, M.; Bailey, C.; Genevicius, K.; Shkunov, M.; Sparrowe, D.; Tierney, S.; McCulloch, I. *J. Am. Chem. Soc.* **2005**, *127*, 1078–1079. (e) Li, Y.; Wu, Y.; Liu, P.; Birau, M.; Pan, H.; Ong, B. S. *Adv. Mater.* **2006**, *18*, 3029–3032. (f) Usta, H.; Lu, G.; Facchetti, A.; Marks, T. J. *J. Am. Chem. Soc.* **2006**, *128*, 9034–9035. (g) Zhang, M.; Tsao, H. N.; Pisula, W.; Yang, C.; Mishra, A. K.; Müllen, K. *J. Am. Chem. Soc.* **2007**, *129*, 3472–3473. (h) Pan, H.; Li, Y.; Liu, P.; Ong, B. S.; Zhu, S.; Xu, G. *J. Am. Chem. Soc.* **2007**, *129*, 4112–4113. (i) McCulloch, I.; Heeney, M.; Bailey, C.; Genevicius, K.; Macdonald, I.; Shkunov, M.; Sparrowe, D.; Tierney, S.; Wagner, R.; Zhang, W.; Chabinyc, M. L.; Kline, R. J.; McGehee, M. D.; Toney, M. F. *Nat. Mater.* **2006**, *5*, 328–333. (j) Ong, B. S.; Wu, Y.; Li, Y.; Liu, P.; Pan, H. *Chem. Eur. J.* **2008**, *14*, 4766–4778.
(4) Arias, A. C.; Endicott, F.; Street, R. A. *Adv. Mater.* **2006**, *18*, 2900–2904.
(5) Hamadani, B. H.; Gundlach, D. J.; McCulloch, I.; Heeney, M. *Appl. Phys. Lett.* **2007**, *91*, 243512.
(6) (a) Herwig, P. T.; Müllen, K. *Adv. Mater.* **1999**, *11*, 480–483. (b) Mushrush, M.; Facchetti, A.; Lefenfeld, M.; Katz, H. E.; Marks, T. J. *J. Am. Chem. Soc.* **2003**, *125*, 9414–9423. (c) Murphy, A. R.; Fréchet, J. M. J.; Chang, P.; Lee, J.; Subramanian, V. *J. Am. Chem. Soc.* **2004**, *126*, 1596–1597. (d) Aramaki, S.; Sakai, Y.; Ono, N. *Appl. Phys. Lett.* **2004**, *84*, 2085–2087.
(7) (a) Anthony, J. E.; Brooks, J. S.; Eaton, D. L.; Parkin, S. R. *J. Am. Chem. Soc.* **2001**, *123*, 9482–9483. (b) Sheraw, C. D.; Jackson, T. N.; Eaton, D. L.; Anthony, J. E. *Adv. Mater.* **2003**, *15*, 2009–2011. (c) Payne, M. M.; Parkin, S. R.; Anthony, J. E.; Kuo, C.-C.; Jackson, T. N. *J. Am. Chem. Soc.* **2005**, *127*, 4986–4987. (d) Dickey, K. C.; Anthony, J. E.; Loo, Y.-L. *Adv. Mater.* **2006**, *18*, 1721–1726. (e) Park, S. K.; Jackson, T. N.; Anthony, J. E.; Mourey, D. A. *Appl. Phys. Lett.* **2007**, *91*, 063514. (f) Anthony, J. E. *Angew. Chem., Int. Ed.* **2008**, *47*, 452–483.
(8) Ebata, H.; Izawa, T.; Miyazaki, E.; Takimiya, K.; Ikeda, M.; Kuwabara, H.; Yui, T. *J. Am. Chem. Soc.* **2007**, *129*, 15732–15733.
(9) Izawa, T.; Miyazaki, E.; Takimiya, K. *Adv. Mater.* **2008**, *20*, 3388–3392.
(10) (a) Yamada, K.; Okamoto, T.; Kudoh, K.; Wakamiya, A.; Yamaguchi, S.; Takeya, J. *Appl. Phys. Lett.* **2007**, *90*, 072102. (b) Kim, Y. M.; Lim, E.; Kang, I. N.; Jung, B. J.; Lee, J.; Koo, B. W.; Do, L. M.; Shim, H. K. *Macromolecules* **2006**, *39*, 4081–4085. (c) Okamoto, T.; Kudoh, K.; Wakamiya, A.; Yamaguchi, S. *Org. Lett.* **2005**, *7*, 5301–5304. (d) Takimiya, K.; Kunugi, Y.; Konda, Y.; Ebata, H.; Toyoshima, Y.; Otsubo, T. *J. Am. Chem. Soc.* **2006**, *128*, 3044–3050. (e) Takimiya, K.; Kunugi, Y.; Konda, Y.; Niihara, N.; Otsubo, T. *J. Am. Chem. Soc.* **2004**, *126*, 5084–5085. (f) Kunugi, Y.; Takimiya, K.; Yamane, K.; Yamashita, K.; Aso, Y.; Otsubo, T. *Chem. Mater.* **2003**, *15*, 6–7. (g) Crouch, D. J.; Skabara, P. J.; Lohr, J. E.; McDouall, J. J. W.; Heeney, M.; McCulloch, I.; Sparrowe, D.; Shkunov, M.; Coles, S. J.; Horton, P. N.; Hursthouse, M. B. *Chem. Mater.* **2005**, *17*, 6567–6578. (h) Yamamoto, T.; Takimiya, K. *J. Am. Chem. Soc.* **2007**, *129*, 2224–2225.
(11) (a) Aqad, E.; Lakshmikantham, M. V.; Cava, M. P. *Org. Lett.* **2001**, *3*, 4283–4285. (b) Pang, H.; Skabara, P. J.; Gordeyev, S.; McDouall, J. J. t.; Coles, S. J.; Hursthouse, M. B. *Chem. Mater.* **2007**, *19*, 301–307. (c) Patra, A.; Wijsboom, Y. H.; Zade, S. S.; Li, M.; Sheynin, Y.; Leitus, G.; Bendikov, M. *J. Am. Chem. Soc.* **2008**, *130*, 6734–6736.
(12) *Organoselenium Chemistry*; Back, T. G. Ed.; Oxford University Press: Oxford, 1999.

Scheme 1. Efficient Two-Step Synthesis of Parent BSBS and 2,7-Diphenyl Derivative

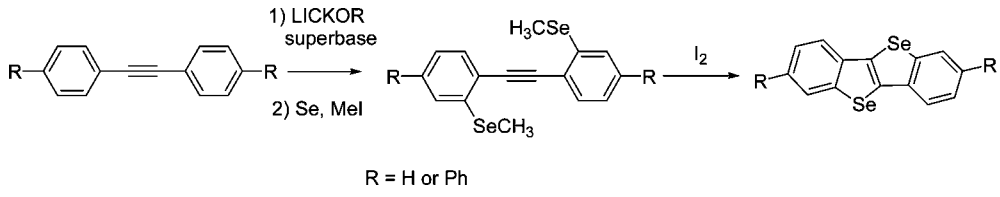

Scheme 2. Synthesis of C_{12}-BSBS via Modified Routes

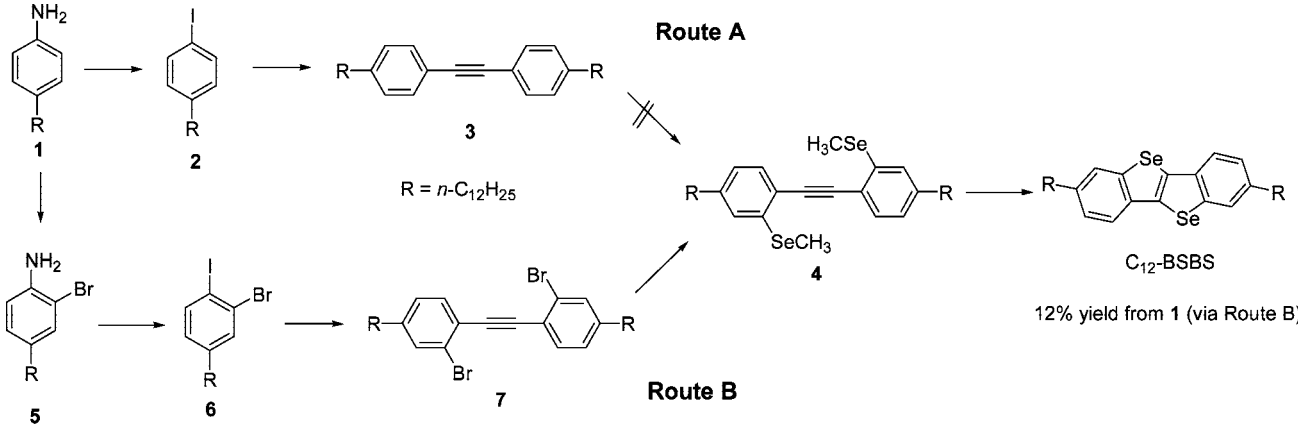

Scheme 3. Improved Synthesis of Parent BSBS and Synthesis of C_n-BSBSs via 2,7-Dibromo-BSBS

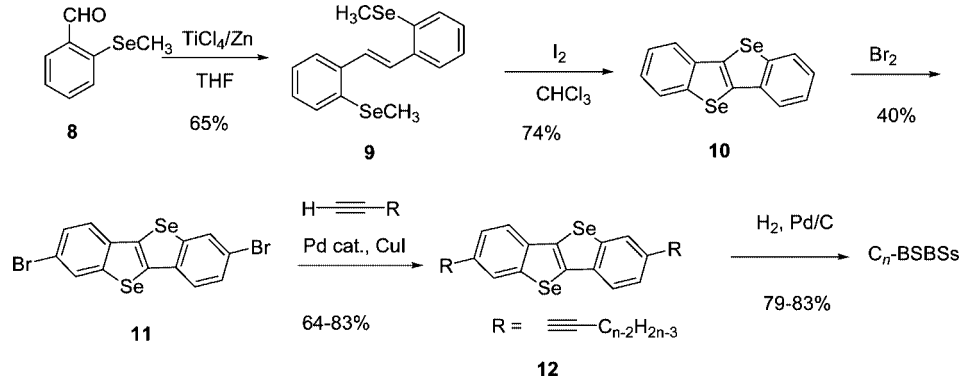

byproduct of the reaction between *o*-methylselenobenzaldehyde and bromoacetic acid.[13] An improved synthesis of BSBS was reported by Sashida and Yasuike.[14] We also developed a straightforward two-step procedure for the syntheses of BSBS and its 2,7-diphenyl derivative from easily available diphenyl acetylenes with the LICKOR superbase,[15] followed by subsequent reactions with selenium powder and methyl iodide to give 2,2′-bis(methylseleno)diphenyl acetylenes, which were readily converted into the BSBS derivatives (Scheme 1).[10d]

For the synthesis of C_n-BSBSs, we examined first the two-step procedure from the diphenyl acetylene derivatives, primarily because of the accessibility of the precursor, 4,4′-dialkyldiphenyl acetylene. Using commercially available *p*-dodecylaniline (**1**) as the starting material, 4,4′-didodecyldiphenyl acetylene (**3**) was synthesized as the key intermediate for C_{12}-BSBS (Scheme 2, Route A).[16] Treatment of **3** with the LICKOR superbase followed by the subsequent addition of selenium powder and methyl iodide, however, resulted in almost quantitative recovery of **3**. To circumvent the poor reactivity of **3** in the direct *o*-lithiation reaction, we next examined Route B in Scheme 2, where 2,2′-dibromo-4,4′-didodecyldiphenyl acetylene (**7**) was chosen as the precursor for the synthesis of 2,2′-bis(methylseleno)-4,4′-didodecyldiphenyl acetylene (**4**).

After selective *o*-bromination of **1** with *N*-bromosuccinimide (NBS) to give **5** in 70% yield, diazotization of the amino group in **5** followed by a reaction with potassium iodide gave the desired **6** in approximately 60% yield. However, the product was contaminated with 3-dodecylbromobenzene (~15% yield as estimated from the ^{1}H NMR spectra, Figure S1, Supporting Information), which could not be removed completely. The subsequent Sonogashira coupling reaction with trimethylsilylacetylene using contaminated **6** gave **7** as a white powder. Repeated chromatographic purifications and recrystallizations of the product could not yield analytically pure **7** (judging from the ^{1}H NMR spectra, ca. 90% pure, Figure S2, Supporting Information), owing to the byproduct originating from 3-dodecylbromobenzene. Treatment of the product with ^{t}BuLi followed by a reaction

(13) Faller, P.; Mantovani, F. *Bull. Soc. Chim. France* **1972**, 1643–1645.
(14) Sashida, H.; Yasuike, S. *J. Heterocyclic Chem.* **1988**, *35*, 725–726.
(15) Kowalik, J.; Tolbert, L. M. *J. Org. Chem.* **2001**, *66*, 3229–3231.
(16) Kitamura, T.; Abe, T.; Fujiwara, Y.; Yamaji, T. *Synthesis* **2003**, 213–216.

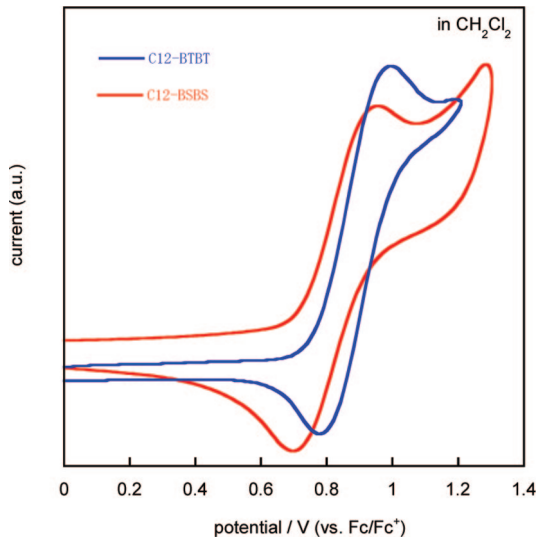

Figure 3. Cyclic voltammograms of C_{12}-BTBT and C_{12}-BSBS.

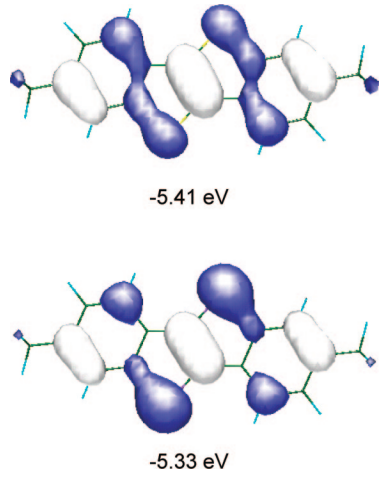

Figure 4. HOMOs of C_1-BTBT and C_1-BSBS calculated with DFT at B3LYP-6-31g(d) level.

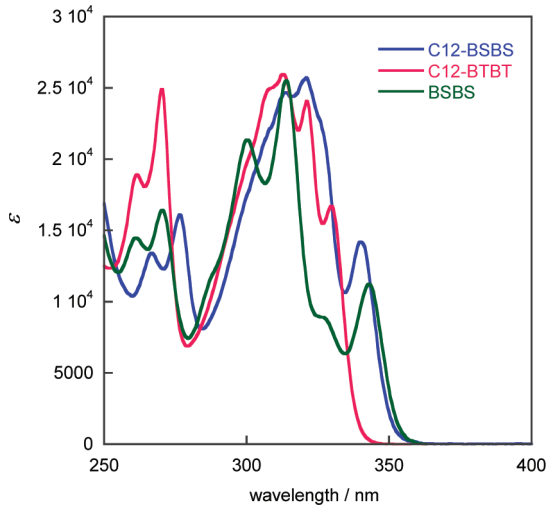

Figure 5. UV−vis spectra of C_{12}-BTBT, C_{12}-BSBS, and parent BSBS.

with selenium powder and methyl iodide gave bis(methylseleno) precursor (**4**). Subsequent reaction of **4** with iodine in refluxing chloroform gave the desired product, and at this stage, the product, C_{12}-BSBS, could be analytically purified by column chromatography and recrystallization. Although the present method produced C_{12}-BSBS in 12% total yield from **1**, it has drawbacks, including the problematic purification of **6** and the need of individual starting materials for C_n-BSBSs with different alkyl groups. For these reasons, we sought another synthetic route via a common intermediate, that is, 2,7-dihalobenzoselenophenobenzoselenophene.

Since a preliminary experiment that involved bromination of the parent BSBS gave 2,7-dibromo derivative (**11**), we next planned to introduce alkyl groups to the BSBS core via **11**. In this synthetic strategy, the preparation of a large amount of parent BSBS is the key issue. Neither Sashida and Yasuike's method nor our previously developed method (Scheme 1) was amenable to the large-scale synthesis because of the requirement of precise control of reaction temperature at the metalation steps, and either method resulted in low reproducibility particularly when conducted in multigram scale. Therefore, we reinvestigated new potential synthetic methods for BSBS and found that 2-methylselenobenzaldehyde (**8**), which is easily accessible from methyl anthranilate,[17] can be effectively converted into BSBS via the low-valent titanium-mediated olefination to give *trans*-2,2′-bis(methylseleno)stilbene (**9**), and this was followed by demethylation-ring closing reaction effected by iodine (Scheme 3).[10h] Bromination of BSBS with bromine gave 2,7-dibromo-BSBS (**11**) in 40% isolated yield after repeated recrystallizations from chlorobenzene. Palladium-catalyzed Sonogashira coupling reaction with various terminal acetylenes gave bis(alkyne) derivatives (**12**) in 64−83% isolated yield, and **12** was readily converted into the desired C_n-BSBSs by hydrogenation in the presence of Pd/C (Scheme 3). The present synthetic method is advantageous in terms of the versatility of the synthesis of C_n-BSBSs with different alkyl substituents.[18] All the C_n-BSBSs were fully characterized by spectroscopic and combustion elemental analyses.

As expected, C_n-BSBSs were highly soluble in various organic solvents: the solubilities, which were determined as the saturated concentration in chloroform solution at room temperature were >500, 180, 70, and 30 g L^{-1} for C_8-, C_{10}-, C_{12}-, and C_{14}-BSBSs, respectively. Interestingly, the solubilities are fairly higher than those of corresponding C_n-BTBTs possessing the same alkyl groups. Such high solubilities of C_n-BSBSs made them suitable for solution deposition of thin films.

Physicochemical Properties. All the C_n-BSBSs showed a set of reversible oxidation peaks in cyclic voltammetry measurements (Figure 3). All of them had an oxidation potential ($E^{1/2}_{ox}$) of +0.82 V (vs Fc/Fc^+) within experimental error, which is fairly lower than that of the parent BSBS (+1.06 V), reflecting the electron-donating nature of the introduced alkyl groups. Compared with the oxidation potentials of C_n-BTBTs (+0.89 V), it is reasonable to consider that C_n-BSBSs have slightly higher energy levels of the highest occupied molecular orbitals (HOMOs) than C_n-BTBTs (Figure 3). The HOMO energy level estimated from the oxidation onset (+0.71 V vs Fc/Fc^+) was ca. 5.51

(17) Iwaoka, M.; Komatsu, H.; Katsuda, T.; Tomoda, S. *J. Am. Chem. Soc.* **2004**, *126*, 5309–5317. See also Supporting Information for details. .
(18) With **11** and phenyl boronic acid, 2,7-diphenyl derivative (DPh-BSBS) was also synthesized under Suzuki coupling conditions.

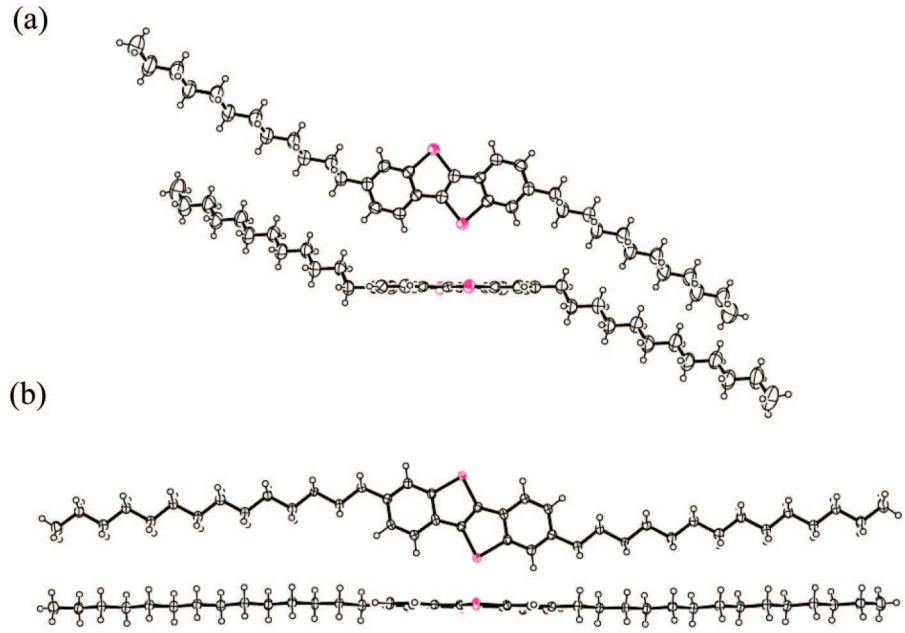

Figure 6. Molecular structures of C_{12}-BSBS (a) and C_{14}-BSBS (b).

Table 1. Crystallographic Parameters of C_8-, C_{10}-, C_{12}-, and C_{14}-BSBSs

	C_8-BSBS	C_{10}-BSBS	C_{12}-BSBS	C_{14}-BSBS
empirical formula	$C_{30}H_{40}Se_2$	$C_{34}H_{48}Se_2$	$C_{38}H_{56}Se_2$	$C_{42}H_{64}Se_2$
formula weight	558.57	614.67	670.78	726.89
crystal color, habit	colorless, block	colorless, block	colorless, block	colorless, block
crystal dimensions, mm^3	0.50 × 0.30 × 0.30	0.50 × 0.30 × 0.30	0.65 × 0.30 × 0.15	0.80 × 0.80 × 0.10
crystal system	monoclinic	monoclinic	monoclinic	monoclinic
a, Å	56.717(6)	5.614(1)	74.52(1)	5.5648(6)
b, Å	4.1874(5)	7.296(2)	4.4014(7)	7.3316(8)
c, Å	11.189(1)	36.00(1)	10.693(3)	45.334(4)
β, deg	94.912(3)	92.88(1)	94.500(3)	93.289(3)
V, $Å^3$	2647.7(5)	1472(2)	3496(10)	1746.5(3)
space group	$C2/c$ (No. 15)	$P2_1/n$ (No. 14)	$C2/c$ (No. 15)	$P2_1/c$ (No. 14)
Z value	4	2	4	2
temperature, K	170	100	293	170
no. of reflections measured	13016	11687	8795	16324
no. of reflections ($I > 2\sigma$)	2322	2542	2036	3035
no. of variables	145	163	181	199
residuals: R; wR^2	0.071; 0.178	0.052; 0.088	0.070; 0.145	0.058, 0.153
goodness of fit indicator	3.32	1.17	1.45	1.052

eV below the vacuum level,[19] which is fairly consistent with the HOMO energy level of virtual C_1-BSBS (5.33 eV below the vacuum level) calculated with the DFT method at the B3LYP-6-31g(d) level as the model compound.[20] The MO calculation reproduced the effects of incorporated chalcogen atoms on the HOMO energy level: the calculated energy level of C_1-BTBT is 5.40 eV, which is slightly lower than that of C_1-BSBS (Figure 4).

The UV−vis spectrum of C_{12}-BSBS is shown in Figure 5 together with those of the parent BSBS and C_{12}-BTBT for comparison. The introduction of alkyl groups brought about changes in the absorption band around 300−330 nm but no distinct difference in the absorption edge. In contrast, the substitution of sulfur atoms with selenium atoms caused a red shift of the absorption edge. The estimated HOMO−lowest unoccupied molecular orbital (LUMO) gap of C_{12}-BSBS from the absorption edge is approximately 3.5 eV, which is slightly smaller than that of C_{12}-BTBT (ca. 3.6 eV). We also measured the UV−vis spectrum of C_{12}-BSBS in air-saturated CH_2Cl_2 solution (Figure S4, Supporting Information). The spectrum was not changed at all even after 72 h, demonstrating the high air stability of C_n-BSBSs.

From these physicochemical characterizations, we conclude that the electronic properties, solubilities, and stabilities of C_n-BSBSs are very similar to those of their sulfur counterparts, C_n-BTBTs, indicating that the selenium substitution does not significantly change the nature of the π-electron system.

Molecular and Crystal Structures of C_n-BSBSs. Single-crystal X-ray analysis confirmed the successful syntheses of all C_n-BSBSs (n = 8, 10, 12, 14). The crystallographic parameters listed in Table 1 show that they are crystallographically classified into two groups: one includes C_8- and C_{12}-BSBSs with the *monoclinic* space group and the body-centered cell (designated as crystal A phase), and the other

(19) (a) Brédas, J.-L.; Silbey, R.; Boudreaux, D. S.; Chance, R. R. *J. Am. Chem. Soc.* **1983**, *105*, 6555–6559. (b) Pommerehne, J.; Vestweber, H.; Guss, W.; Mark, R. F.; Bässler, H.; Porsch, M.; Daub, J. *Adv. Mater.* **1995**, *7*, 551–554.
(20) Frisch, M. J.; et al. *Gaussian 03*, revision C.02; Gaussian, Inc.: Wallingford, CT, 2004.

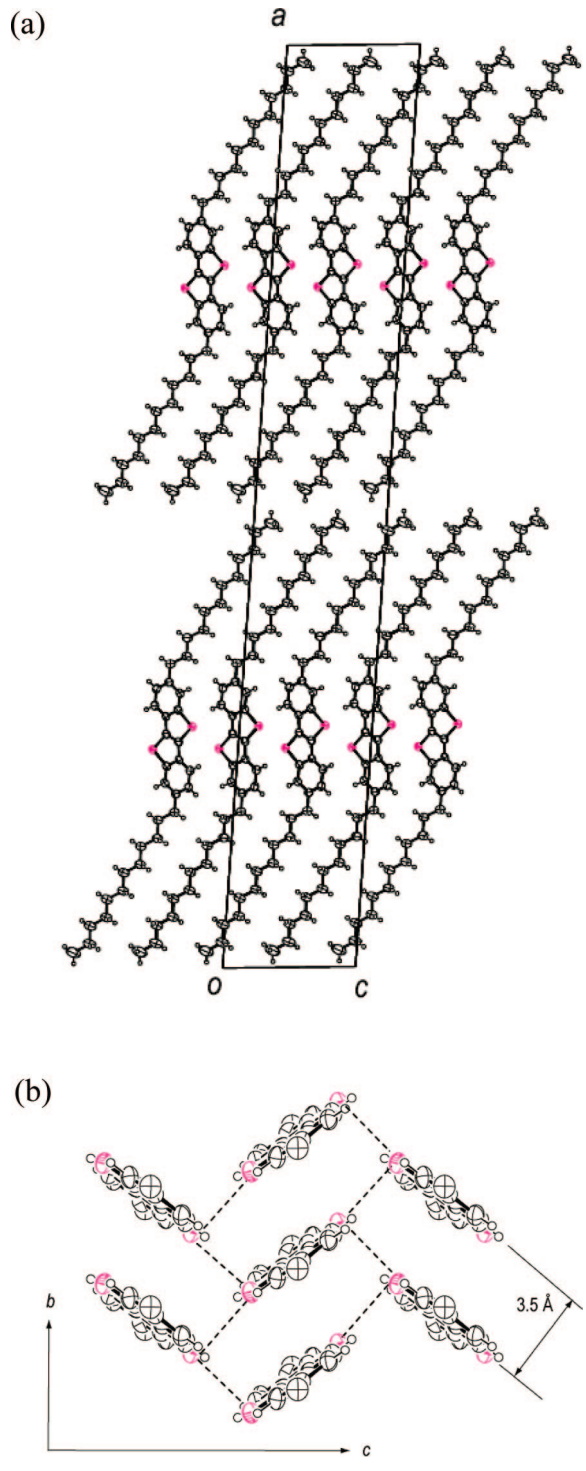

Figure 7. (a) Crystal structure of C_{12}-BSBS (*b*-axis projection). (b) Molecular arrangement of BSBS cores in C_{12}-BSBS (*a*-axis projection).

includes C_{10}- and C_{14}-BSBSs with the *monoclinic* space group and the primitive cell (designated as crystal B phase). In accordance with the different crystallographic parameters, their molecular and crystal structures differ from each other. The molecules of C_8- and C_{12}-BSBSs (crystal A phase) assume stretched, doubly bent structures in which the alkyl groups (*n*-octyl or *n*-dodecyl groups) have a staggered, all-*anti* conformation that minimizes steric energy in the aliphatic chains (Figure 6a). In contrast, *n*-decyl and *n*-tetradecyl groups in C_{10}- and C_{14}-BSBSs (crystal B phase), similarly taking the all-*anti* conformation, lie on the same plane as the BSBS core, resulting in fairly flat molecular structures (Figure 6b). The latter structure most likely minimizes the space required, allowing dense packing in bulk crystals.

The molecular arrangement of each phase is also distinctly different: in the crystal A phase (C_8- and C_{12}-BSBSs), the molecular long axis is almost parallel to the crystallographic *a*-axis and the BSBS core layer and two layers of alkyl chain parts are stacked alternately along the *a*-axis direction, forming an infinite lamella-like structure (Figure 7a). Since two molecular layers are in the crystallographic unit cell, the *a*-axes are almost twice the molecular length, resulting in a highly anisotropic unit cell particularly for C_{12}-BSBS, whose *a*-axis is 74.5 Å long, whereas the *b*-axis is approximately 4.4 Å. The ratio of *a*/*c* is approximately 17 and is, to our knowledge, one of the most anisotropic unit cells ever reported for organic compounds.[21]

In the BSBS core layers, the molecular arrangement has the face-to-face π-stacking structure with an interplane distance of 3.54 Å. Although no nonbonded Se−Se distance shorter than the sum of the van der Waals radii (3.8 Å) was observed in the π-stacks, fairly short Se−Se contacts (3.54 Å) between π-stacks were observed (Figure 7b).

The present packing structure is somewhat different from those of C_n-BTBTs, whose molecular arrangements are characterized as the herringbone type with a two-dimensional (2D) electronic nature. Although generally speaking, the electronic nature of the face-to-face π-stacking structure tends to be anisotropic and one-dimensional,[21] the present structure likely has the 2D electronic nature as a p-channel organic semiconductor, because of the existence of nonbonded Se−Se contacts. DFT-MO calculations of the BSBS derivatives (vide supra) showed that large charge densities (orbital coefficients) reside on the selenium atoms in the HOMO. Therefore, the intermolecular overlap of HOMOs through the Se−Se contacts together with the π-stacking is expected to be effective for the formation of an isotropic 2D electronic structure. Because of the molecular arrangement that enables the 2D structure, C_n-BSBSs, provided that the present molecular arrangement is realized in the thin film state, will be promising organic semiconductors for high-performance OFETs. This contrasts with the electronic structure of π-stacking pentathienoacene whose HOMO has nodes on the sulfur atoms, diminishing the overlap of HOMOs between neighboring π-stacks and making the electronic nature of pentathienoacene-based solid highly anisotropic (1D) as a p-channel organic semiconductor.[22a,23]

Another type of molecular arrangement was observed for C_{10}- and C_{14}-BSBSs with the *monoclinic* space group and the primitive cell (crystal B phase). Similar to the former

(21) Hotta, S.; Goto, M.; Azumi, R.; Inoue, M.; Ichikawa, M.; Taniguchi, Y. *Chem. Mater.* **2004**, *16*, 237–241.
(22) (a) Kim, E. G.; Coropceanu, V.; Gruhn, N. E.; Sanchez-Carrera, R. S.; Snoeberger, R.; Matzger, A. J.; Brédas, J. L. *J. Am. Chem. Soc.* **2007**, *129*, 13072–13081. (b) Kashiki, T.; Miyazaki, E.; Takimiya, K. *Chem. Lett.* **2008**, *37*, 284–285.
(23) Xiao, K.; Liu, Y.; Qi, T.; Zhang, W.; Wang, F.; Gao, J.; Qiu, W.; Ma, Y.; Cui, G.; Chen, S.; Zhan, X.; Yu, G.; Qin, J.; Hu, W.; Zhu, D. *J. Am. Chem. Soc.* **2005**, *127*, 13281–13286.

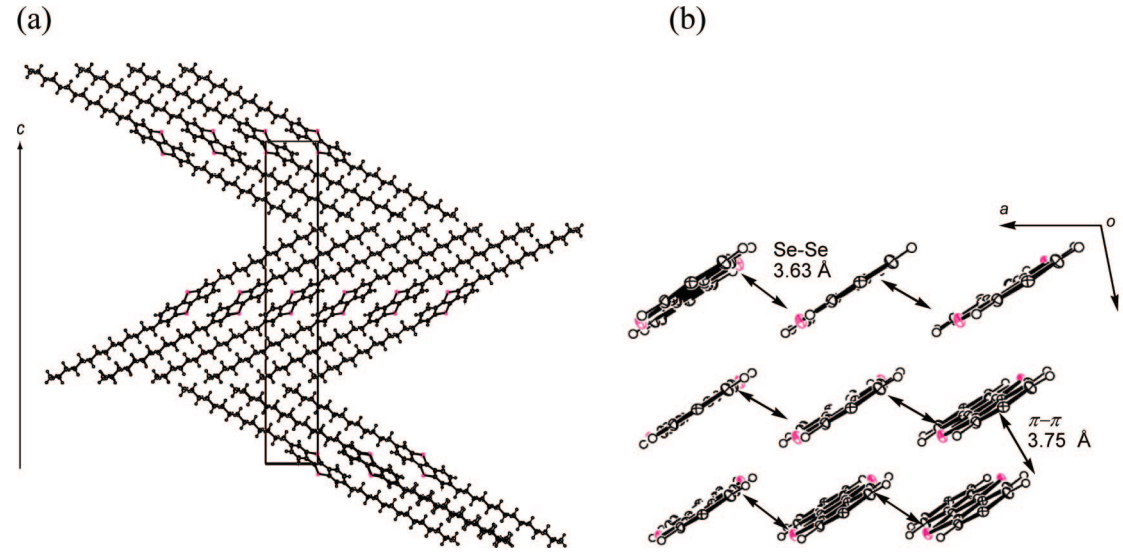

Figure 8. (a) Crystal structure (*a*-axis projection) and (b) molecular arrangement of BSBS cores in C_{14}-BSBS (*c*-axis projection).

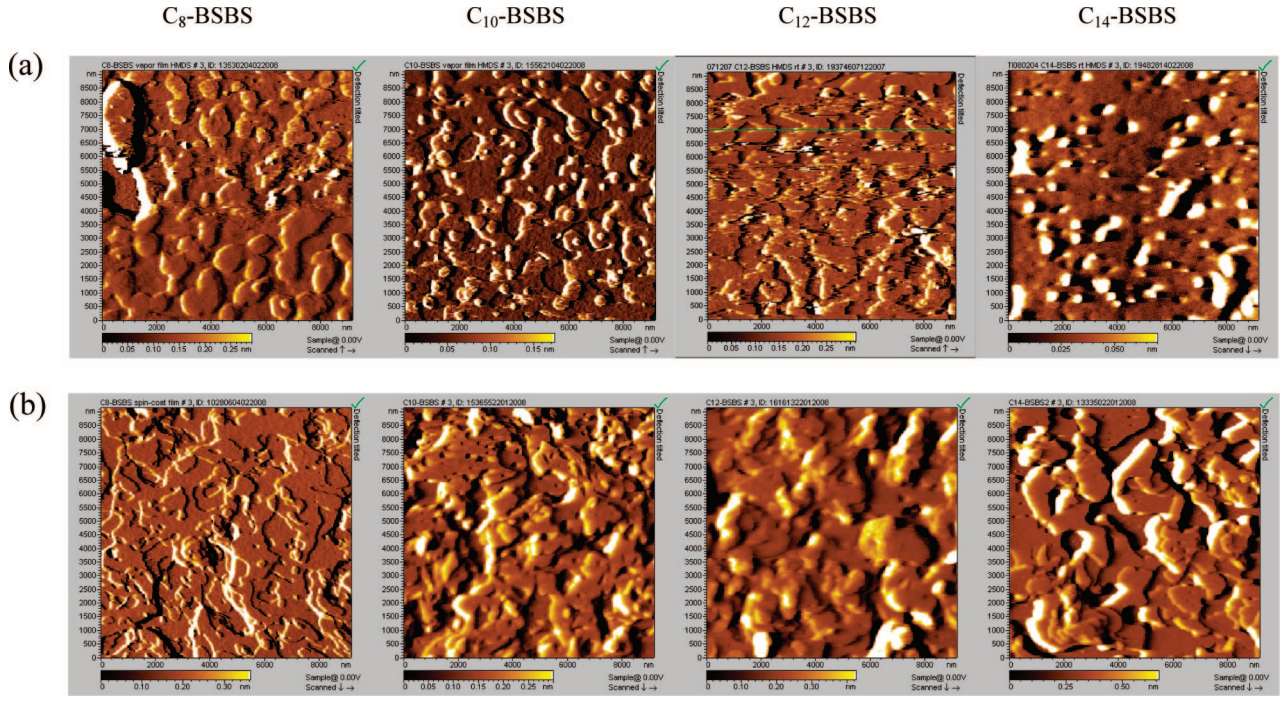

Figure 9. AFM images of (a) vapor-deposited thin films on HDMS-treated Si/SiO_2 substrates and (b) spin-coated thin films on bare Si/SiO_2 substrates.

group, C_n-BSBS molecules are packed in the lamella-like layer-by-layer structure along the *c*-axis direction, but the molecular long axes largely tilt from the *c*-axis (Figure 8a). Thus, the arrangement of BSBS core parts in each layer is quite different from those of C_8- and C_{12}-BSBSs. At first glance, the structure looks like a face-to-face π-stack along the *b*-axis direction (Figure 8b), but a large slip along the molecular long axis direction and the long face-to-face distance (3.75 Å) make the molecular overlap in this direction less effective. On the other hand, short intermolecular Se−Se contacts (<3.7 Å) creating a "ribbon-like" molecular array were observed along the *a*-axis direction, implying that the overlap between the molecules in the present crystal packing is highly anisotropic and not very effective.

Thin Films. The deposition of thin films by both physical vapor deposition and spin-coating of chloroform solution was

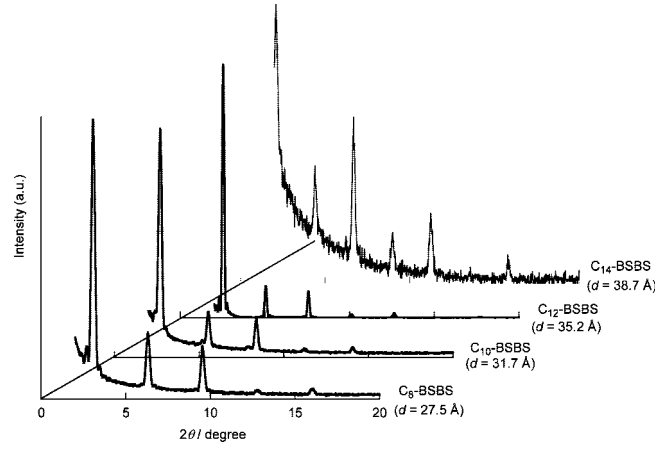

Figure 10. XRD patterns of vapor-deposited thin films of C_n-BSBSs.

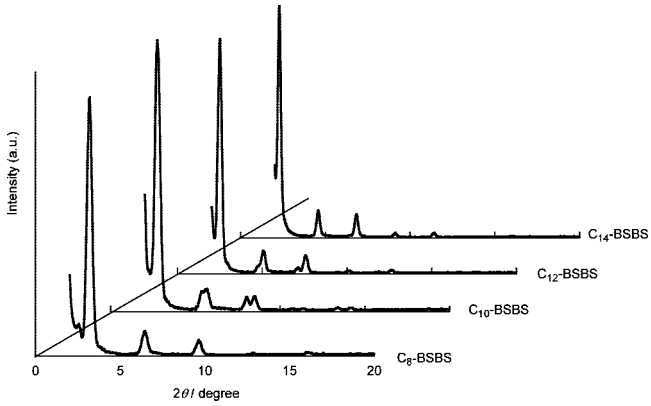

Figure 11. XRD patterns of spin-coated thin films of C_n-BSBSs.

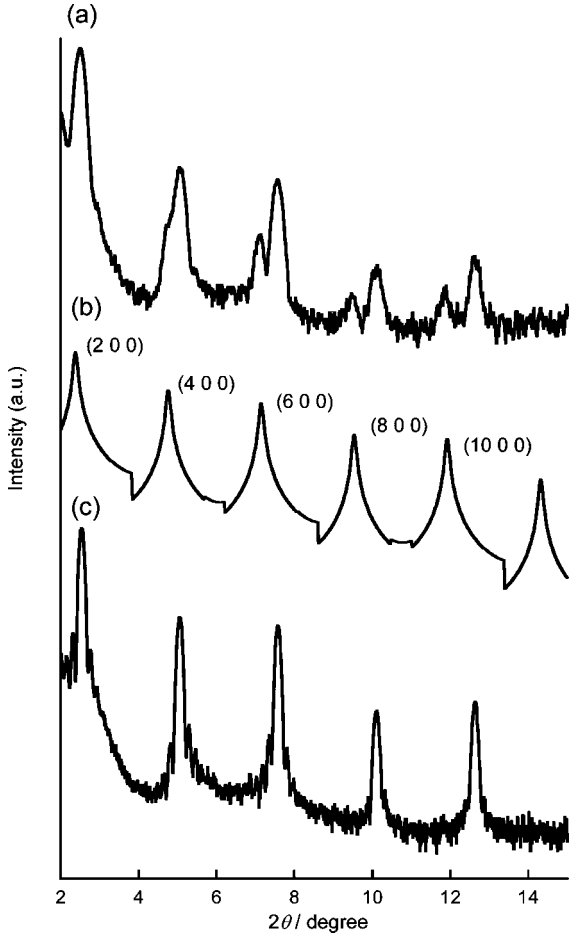

Figure 12. Comparison of XRD patterns of C_{12}-BSBS: (a) spin-coated film, (b) simulated powder pattern of bulk single crystal, and (c) vapor-deposited film.

examined, and both methods gave similar homogeneous films on Si/SiO_2 substrates. During vapor deposition, C_n-BSBSs melted first in the source owing to their low melting points and then evaporated. The obtained thin films, however, appeared homogeneous with a metallic luster on the surface. AFM images (Figure 9a) show that the films consist of crystalline grains of submicrometer to several micrometers in size, as seen in many vapor-deposited thin films of conventional molecular organic semiconductors. However, the grain boundaries are not clearly seen, implying good connectivity between the grains. Similar film morphologies were observed for the spin-coated films (Figure 9b).

XRD Measurements. XRD measurements indicated that the films have crystalline order in the direction of the substrate normal. As illustrated in Figure 10, all the vapor-deposited films show a series of peaks well characterized as a series of (00*l*) diffractions with one interlayer distance (*d*-spacing). The peaks, however, cannot be assigned to the bulk single-crystal phases: neither (*h*00) nor (00*l*) peaks in the simulated powder patterns of C_8- and C_{12}- (crystal A phase) or C_{10}- and C_{14}-BSBSs (crystal B phase) based on the bulk single crystals correspond to the peaks in the thin film XRDs. We thus conclude that the vapor-deposited thin films have a distinct phase ("thin film phase"). Since the increment of *d*-spacings is almost constant (3.5−4.2 Å per ethylene unit) with the elongation of alkyl chains, C_n-BSBS molecules are speculated to take a similar molecular orientation on the substrate in the thin film phase.

The XRD patterns of spin-coated thin films (Figure 11) are almost identical with those of vapor-deposited films: a series of (00*l*) peaks assigned to the same *d*-spacings were observed in the XRD patterns of C_8- and C_{14}-BSBS films, whereas the XRD patterns of C_{10}- and C_{12}-BSBS films had two different series of peaks. In Figure 12 that shows the XRD pattern of the spin-coated film of C_{12}-BSBS as representative, weak but distinct peaks assignable to the crystal phase (crystal A phase) together with major peaks assignable to the thin film phase were observed. Although peaks in the low 2θ regime overlapped with those from the thin film phase, (6 0 0), (8 0 0), and (10 0 0) peaks from the crystal A phase were clearly seen. A similar XRD pattern was observed for the spin-coated thin film of C_{10}-BSBS. However, the additional peaks could not be assigned to the bulk single-crystal phase of C_{10}-BSBS (crystal B phase). Therefore, we speculate that the crystal A phase, although not confirmed in the bulk single crystal, appears in the spin-coated thin film of C_{10}-BSBS.

Table 2 summarizes the observed phases of C_n-BSBSs in the solid state (bulk single crystals and thin films). In the present study, we were able to detect at least three different phases that may be energetically competing in the condensed phase of C_n-BSBSs. Although the exact molecular arrangement in the thin film phase was not elucidated, it is reasonable to consider from the *d*-spacings and the molecular lengths that the molecules in the thin film phase also assume a similar molecular arrangement to those in the crystal A phase but with a slightly larger inclination of the molecules from the substrate normal (Figure S5, Supporting Information).

FET Devices. FET devices with the top-contact configuration were fabricated by vapor deposition of gold source and drain electrodes (80 nm) on top of the thin films through a shadow mask that defined the channel length and width of 50 μm and 1.5 mm, respectively. In the case of vapor-processed devices, Si/SiO_2 substrates treated with hexamethyldisilazane (HMDS) were used. All the devices showed typical p-channel FET responses under ambient conditions (Figure 13). The extracted FET parameters are summarized in Table 3.

Comparison of FET characteristics between vapor-processed devices and solution-processed ones revealed that

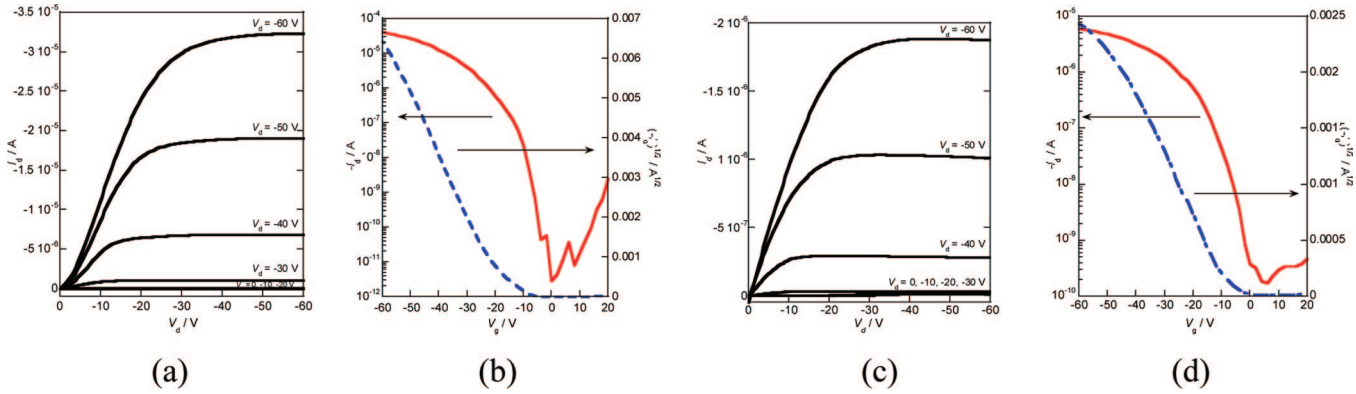

Figure 13. FET characteristics of C_{12}-BSBS-based OFETs: output (a) and transfer curves (b) of vapor-processed device and output (c) and transfer curves (d) of solution-processed device.

Table 2. Classification of Solid-State Phases Observed for C_n-BSBSs

	bulk single crystal		vapor-deposited film		spin-coated film			
					major		minor	
	phase	d, Å	phase	d, Å	phase	d, Å	phase	d, Å
C_8-BSBS	cryst. A	28.3 (a/2)	thin film	27.5	thin film	27.5		
C_{10}-BSBS	cryst. B	18.0 (c/2)	thin film	31.7	thin film	31.7	cryst. A	33.0
C_{12}-BSBS	cryst. A	37.2 (a/2)	thin film	35.2	thin film	35.2	cryst. A	37.1
C_{14}-BSBS	cryst. B	22.8 (c/2)	thin film	38.7	thin film	38.7		

Table 3. FET Performance of C_n-BSBSs[a]

organic layer	compound	μ_{FET}, $cm^2\ V^{-1}\ s^{-1}$	V_{th}, V	I_{on}/I_{off}
vapor-deposited film (HMDS substrate)	C_8-BSBS	0.066	−9.9	10^6
	C_{10}-BSBS	0.18	−13.8	10^6
	C_{12}-BSBS	0.23	−10.3	10^6
	C_{14}-BSBS	0.16	−15.1	10^6
spin-coated film	C_8-BSBS	0.012	−3.5	10^5
	C_{10}-BSBS	0.013	−1.6	5.0×10^4
	C_{12}-BSBS	0.03	−8.8	10^5
	C_{14}-BSBS	0.02	−2.2	10^3

[a] More than 20 devices for each category were tested to confirm reproducibility and parameters were extracted from typical devices.

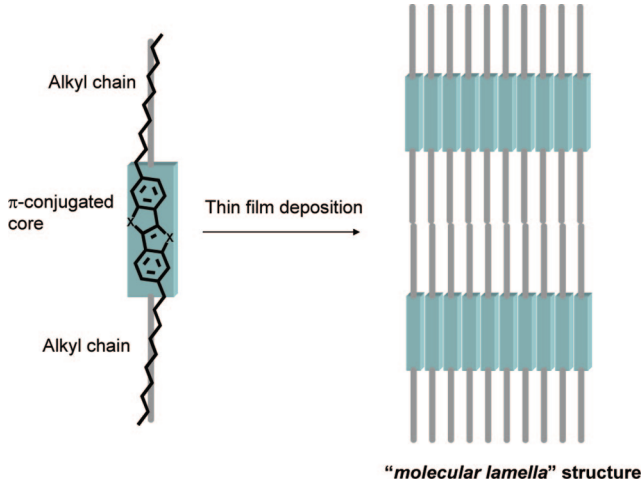

Figure 14. Schematic of self-assembly of C_n-BTBT and C_n-BSBS molecules.

the former tended to show better performance for all derivatives than the latter. The vapor-processed devices with C_n-BSBSs having longer alkyl chains (n = 10, 12, 14) showed μ_{FET} values higher than 0.1 $cm^2\ V^{-1}\ s^{-1}$, whereas μ_{FET} values of the solution-processed devices were one-fifth of or one order of magnitude lower than those of the vapor-processed devices.

The low mobilities of the solution-processed devices could be related to the quality of the films: detailed comparison of the XRD patterns of vapor-deposited films with those of spin-coated films showed that the former has better crystallinity than the latter, as judged from the sharpness of the peaks (Figure 12). In addition, in the case of C_{10}- and C_{12}-BSBSs, the XRD patterns clearly indicated the coexistence of two phases in the spin-coated films (Figures 11 and 12), demonstrating the reduced uniformity in the transistor channels in solution-processed devices.

Discussion

At the beginning of this study, we expected that the substitution of sulfur atoms in the C_n-BTBT framework with selenium atoms will minimize perturbation of the electronic nature of the molecules yet substantially enhance intermolecular interaction owing to the large atomic radii of selenium atoms and the high polarizability at the molecular periphery, which will bring about improvements in device performance.

Comparison of the physicochemical data of C_n-BSBSs with those of C_n-BTBTs indicated that their electronic natures as π-electron systems are very similar to each other, as expected. On the other hand, their packing structures are significantly different: instead of the unique "2D interactive structure" that realizes high-performance OFET channels observed for C_n-BTBTs, three different solid-state phases, that is, the crystal A phase, the crystal B phase, and the thin film phase, were observed for C_n-BSBSs. Although the exact molecular arrangement of the thin film phase that directly relates to thin film transistors was not determined, the relatively large inclination of the molecular long axis from the substrate normal indicates that the intermolecular overlap between BSBS cores is less favorable than that for the 2D interactive structure in C_n-BTBTs.

In accordance with the molecular arrangement in the thin film phase, the FET performance of the present C_n-BSBS-based devices is inferior to that of C_n-BTBTs: for the vapor-processed devices, the mobilities of C_n-BSBS-based devices (~ 0.2 cm^2 V^{-1} s^{-1}) are less than one-tenth of those of C_n-BTBTs (~ 4.0 cm^2 V^{-1} s^{-1}), and for the solution-processed devices, the mobilities are approximately 2 orders of magnitude lower (C_n-BSBS-based devices, ~ 0.03 cm^2 V^{-1} s^{-1}; C_n-BTBT-based devices, ~ 2.7 cm^2 V^{-1} s^{-1}). These significant decreases of device performance strongly indicate that carrier transport is a physicochemical outcome of the molecular solid, where intermolecular interaction plays an important role.

Another point that should be addressed is the self-assembling tendency of C_n-BTBT and C_n-BSBS molecules. We suppose that their molecular structures are expressed as a combination of a rigid π-conjugated core with two long alkyl groups introduced in the molecular long-axis direction (Figure 14). Regardless of the central heteroarene cores, such molecules take the lamella-like structure ("molecular lamella" structure) in the thin film state, where heteroarene core layers and layers of alkyl chain parts are stacked alternately (Figure 14). It should be emphasized that thin films with such a well-ordered molecular lamella structure were easily obtained by physical vapor deposition or solution deposition, and the thus-obtained thin films acted as FET channels that showed μ_{FET} values of at least 10^{-2} cm^2 V^{-1} s^{-1}. For further enhancement of performance as FET channels, however, a molecular arrangement that allows for strong intermolecular interaction and yields an isotropic (2D) electronic structure in the semiconducting π-core layer is required, as was observed for C_n-BTBTs.

In summary, the present results indicate that even subtle molecular modifications, such as the substitution of sulfur atoms with selenium atoms in the same molecular framework, can alter the molecular arrangement in the solid state, resulting in the large difference in performance of thin film devices. Therefore, for the further development of superior organic semiconductors, molecular design strategies that take into account not only the molecular electronic structure but also the electronic structure in the solid state are of great importance.

Acknowledgment. This work was partially supported by a Grant-in-Aid for Scientific Research (No. 20350088) from the Ministry of Education, Culture, Sports, Science and Technology, Japan, and an Industrial Technology Research Grant Program (No. 04A25015) from the New Energy and Industrial Technology Development Organization (NEDO) of Japan. We also thank Nippon Kayaku Co., Ltd., for cooperation in the research.

Supporting Information Available: Experimental details of the synthesis, crystallographic information files (CIF) for C_n-BTBTs, and complete reference 20. This material is available free of charge via the Internet at http://pubs.acs.org.

CM8030126